Interstellar ^{60}Fe in Antarctica

Dominik Koll,[1,*] Gunther Korschinek,[1,2] Thomas Faestermann,[1,2] J. M. Gómez-Guzmán,[1]
Sepp Kipfstuhl,[3] Silke Merchel,[4] and Jan M. Welch[5]

[1]*Physik-Department, Technische Universität München, 85748 Garching, Germany*
[2]*Excellence Cluster Universe, 85748 Garching, Germany*
[3]*Alfred-Wegener-Institut, Helmholtz-Zentrum für Polar- und Meeresforschung, 27568 Bremerhaven, Germany*
[4]*Helmholtz-Zentrum Dresden-Rossendorf, 01328 Dresden, Germany*
[5]*Atominstitut, TU Wien, 1020 Vienna, Austria*

Earth is constantly bombarded with extraterrestrial dust containing invaluable information about extraterrestrial processes, such as structure formation by stellar explosions or nucleosynthesis, which could be traced back by long-lived radionuclides. Here, we report the very first detection of a recent ^{60}Fe influx onto Earth by analyzing 500 kg of snow from Antarctica by accelerator mass spectrometry. By the measurement of the cosmogenically produced radionuclide ^{53}Mn, an atomic ratio of ^{60}Fe/^{53}Mn = 0.017 was found, significantly above cosmogenic production. After elimination of possible terrestrial sources, such as global fallout, the excess of ^{60}Fe could only be attributed to interstellar ^{60}Fe which might originate from the solar neighborhood.

The solar environment is constantly traversed by interplanetary as well as interstellar dust. Interstellar dust has been clearly identified in the Solar System at first by the dust detector onboard the *Ulysses* spacecraft [1]. Extended measurements have been performed by dust detectors onboard the *Galileo* and *Cassini* spacecrafts [2,3] and references therein. It is considered that the origin of the dust is the Local Interstellar Medium (LISM), which consists of several dust containing cloudlets [2]. The two nearest cloudlets around the Solar System are the Local Interstellar Cloud (LIC) and the G-Cloud (Fig. 1). The Solar System is currently on the edge of the LIC, possibly in an overlap region of the LIC and the G-Cloud and will leave the LIC in the next few thousand years; see Refs. [4,5] and references therein. The LISM is a volume with a higher density than the enveloping Local Bubble (LB) [6–8]. The expansion of an adjacent, larger bubble, the Loop I superbubble, could lead to the formation of smaller cloudlets by the interaction with the LB [9]. The LIC might have emerged from this constellation.

The long-lived radionuclide ^{60}Fe ($T_{1/2} = 2.6$ Myr [10,11]) was released by Supernovae (SNe) close to the Solar System and has been found in geological reservoirs, such as deep ocean ferromanganese crusts, nodules, and sediments [12–15] or even in lunar regolith [16] with signatures in the Myr range. The origin of the detected ^{60}Fe was discussed extensively in the past including SNe in the Sco-Cen OB association or in the Tuc-Hor group, where the exact injection or transport mechanisms are still under debate [17–23]. The condensation of ^{60}Fe bearing SN ejecta into dust is in any case essential for the transport into the

Solar System [24]. The detection of a recent ^{60}Fe influx, as predicted by some models [21] or expected by the above outlined origin of the LIC, would help to constrain these models or would establish a link between the source of previously detected ^{60}Fe and the current location of the Solar System within the LISM.
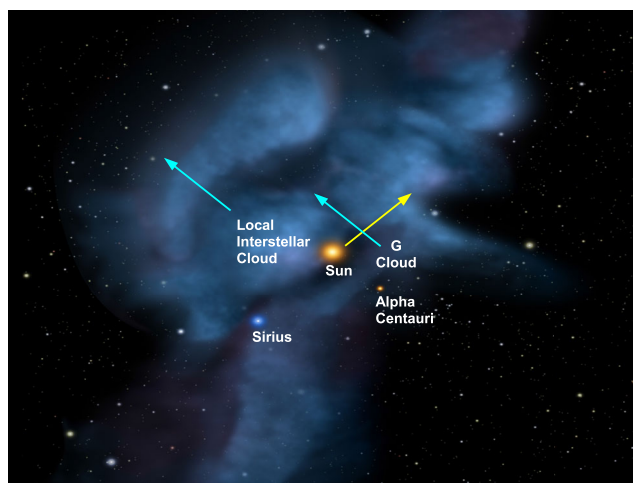

FIG. 1. An illustration of the solar neighborhood and nearby clouds within a distance of about 10 pc. The Solar System is located inside the Local Interstellar Cloud and near the G-Cloud, which are embedded in the larger Local Bubble with a diameter of about 100 pc. The relative motion of the clouds (blue) and the general motion of the Solar System (yellow) are indicated. Figure adapted from NASA/Goddard/Adler/U. Chicago/Wesleyan.

In addition to interstellar dust, interplanetary dust is constantly accreted by Earth. Interplanetary dust particles (IDPs) are released by Solar System objects, like asteroids from the Asteroid Belt or comets, which are considered to contribute most to the interplanetary dust budget on Earth [25]. Interplanetary dust, in contrast to interstellar dust, is slowly moving towards the center of the Solar System by Poynting-Robertson drag after release and is irradiated by solar cosmic rays (SCR) over long timescales. Production rates of radionuclides, such as ^{53}Mn ($T_{1/2} = 3.7$ Myr [26]) or ^{60}Fe, are therefore deducible and depend mostly on the initial elemental composition of the dust particles and to a smaller extent on the object's size for small particles [27]. SCR dominate over galactic cosmic rays (GCR) for the production of long-lived radionuclides in IDPs because of the higher flux inside the Solar System and the particle sizes which do not allow the formation of secondary particle showers within the object [27].

For the search of recent interstellar ^{60}Fe on Earth, an environmental sample with distinct features was necessary to detect smallest concentrations of ^{53}Mn and ^{60}Fe. The sample needs to possess an intrinsic purity concerning the stable isotopes of Mn and Fe as well as the isobars of the isotopes of interest, ^{53}Cr and ^{60}Ni, respectively. Sites with low accumulation or growth rates, resulting in a concentration of the incoming radionuclides, would minimize the initial sample mass. Antarctic surface snow from the German Kohnen Station (75° 00' S, 0° 04' O at 2892 m a.s.l.) was chosen as a suitable material. The Kohnen Station is at a distance of several hundred kilometers from the coastline and on high altitude with an annual accumulation of 80 mm w.e. for recent years [28]. Therefore, any terrestrial input of dust into the sample material could be assumed to be very low. The large mass of 500 kg of Antarctic snow, not older than twenty years, was collected and transported in a frozen state to Munich, Germany. Considering the mean accumulation rate of 80 mm w.e.yr^{-1}, the sample material comprises an active collection area of 6.25 m^2 for one year of precipitation.

The snow was melted and filtered afterwards by cellulose filters with pore sizes of 12–15 μm, followed by cellulose filters with pore sizes of 2–3 μm. By filtration, larger, visible dust particles and micrometeorites could be separated from the rest of the sample material. The filters were incinerated at 650 °C and the ash was chemically treated for element separation at Helmholtz-Zentrum Dresden-Rossendorf based on the prescription in Ref. [29]. The water after filtration was evaporated in a rotary evaporator and afterwards chemically treated at the Atominstitut of TU Wien. Terrestrial stable Fe and Mn were added to both samples as carriers because of the low intrinsic stable Fe and Mn content. For the measurement, the Fe fraction of both, filter and water, samples was obtained, but for the Mn fraction only the filter sample could be used, due to losses during chemistry.

Accelerator mass spectrometry (AMS) is the only measurement technique available at this time to detect the smallest concentrations of ^{53}Mn or ^{60}Fe in the environment. Currently, only two facilities in the world, the Maier-Leibnitz-Laboratory (MLL) of Technical University of Munich and Ludwig Maximilian University of Munich in Garching, Germany and the Heavy Ion Accelerator Facility (HIAF) of The Australian National University in Canberra, Australia achieve sensitivities necessary for the measurement of both isotopes in the ultralow concentration regime. The sensitivity for these radionuclides at the MLL is ^{53}Mn/^{55}Mn $< 10^{-14}$ [30] and ^{60}Fe/Fe $< 10^{-16}$ [15]. For a recent review of the AMS setup at the MLL, see Refs. [31,32].

The uncertainty in these measurements is dominated by the counting statistics of a few events. In this case the 1σ uncertainty intervals of Feldman and Cousins [33] were used to determine the statistical uncertainty. Further statistical uncertainties, which, e.g., include the number of events obtained from the reference material or averaging over measurement sequences, are considerably smaller. The statistical uncertainties were added in quadrature. The only systematic uncertainty in the measurement comes from the uncertainty in concentration of the reference materials, ^{60}Fe/Fe $=(1.3\pm0.3) \times 10^{-12}$, which was produced from and cross-calibrated against the reevaluated primary in-house standard [34,35], and ^{53}Mn/Mn $= (2.8\pm0.1) \times 10^{-10}$ [30].

The measurement of the ^{53}Mn content of the filter residue yielded 12 events of ^{53}Mn. The measured concentration of ^{53}Mn/^{55}Mn $= 3.9^{+1.6}_{-1.4} \times 10^{-13}$ corresponds to 3.0×10^6 atoms of ^{53}Mn with exact knowledge of the stable Mn content after carrier addition for chemistry. The ^{60}Fe measurement of the filter sample was performed in combination with the water sample. Five events of ^{60}Fe were detected in the filter sample. The measured concentration of ^{60}Fe/Fe $= 5.5^{+3.3}_{-2.6} \times 10^{-16}$ corresponds to 5.0×10^4 atoms of ^{60}Fe. Furthermore, in the water sample 5 events that correspond to a concentration of ^{60}Fe/Fe $= 9.1^{+5.4}_{-4.3} \times 10^{-16}$ were detected, yielding 2.3×10^4 atoms of ^{60}Fe in the water because of less carrier addition. The detected concentrations are significantly higher than their corresponding blank level, determined by the measurement of commercial high-purity MnO_2 and Fe_2O_3 powder, and processing blanks, where no background events were recorded in accordance with the established sensitivity (Table I). Combining the results of the water and the filter samples, the total ^{60}Fe deposition in our sample is 7.3×10^4 atoms which could be expressed as an ^{60}Fe influx of 1.2 atoms cm^{-2} yr^{-1}. In the following, only results of the filter sample measurements were used to determine the origin of the detected ^{60}Fe using the radionuclide ratio ^{60}Fe/^{53}Mn.

To trace back the origin of the radionuclide concentrations, either interplanetary or interstellar, we compare

TABLE I. Measured radionuclide ratios in the filter samples by accelerator mass spectrometry. The blank level is given as an 1σ upper limit for 0 counts [33]. Statistical uncertainties are displayed as 1σ upper and lower limits that are dominated by low counting statistics. All blanks used for the measurements are free from the respective radionuclides and yielded no additional background. The measured radionuclide ratios are converted to number of atoms by the knowledge of the stable element content.

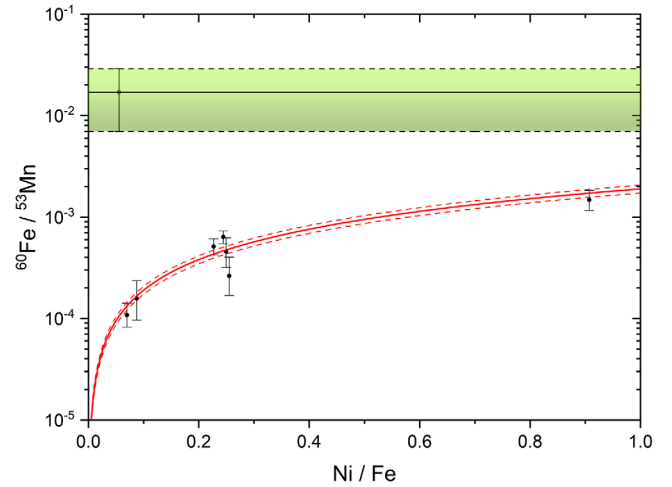|	$^{53}Mn/^{55}Mn$	$^{60}Fe/Fe$	^{53}Mn atoms	^{60}Fe atoms
Filter sample	3.9×10^{-13}	5.5×10^{-16}	3.0×10^{6}	5.0×10^{4}
Upper limit	5.5×10^{-13}	8.8×10^{-16}	4.2×10^{6}	7.9×10^{4}
Lower limit	2.5×10^{-13}	2.9×10^{-16}	1.9×10^{6}	2.6×10^{4}
Blank level	$<1.2 \times 10^{-13}$	$<2.5 \times 10^{-16}$	$\cdots$	$\cdots$

FIG. 2. Atomic $^{60}Fe/^{53}Mn$ ratios for different target element abundances. The red line represents meteoritic ratios [16]. The ratio in Antarctic snow (green) is significantly higher than cosmogenic production for all relevant abundances. Note, the displayed data point is valid for the chondritic abundance of atomic Ni/Fe = 0.055 [37].

them with meteoritic concentrations as described in Ref. [16], in the Supplemental Material to Ref. [16], and references therein [12,36]. There, it was experimentally recognized that for all meteorites the content of ^{60}Fe relative to the respective target element Ni was proportional to the ^{53}Mn content normalized to its main target element Fe, expressed in a $^{60}Fe/Ni$ versus $^{53}Mn/Fe$ plot. In the case of meteorites, stable element abundances could be unambiguously identified as being of extraterrestrial origin. In Antarctic snow, stable element abundances are dominantly of terrestrial origin. A relation to target element abundances accounting for the target-dependent production is therefore not possible for our sample. We convert the meteoritic activity ratios relative to their target elements back to the originally measured atomic concentrations, which also eliminates uncertainties from the half-lives of the radio-nuclides and we evaluate the concentrations as a function of target element abundances (Fig. 2). Abundances up to Ni/Fe = 1 are considered, where the Fe abundance is assumed to dominate over the Ni abundance as is the case for Solar System abundances [37]. The meteoritic data are fitted by $^{60}Fe/^{53}Mn = 0.0019(2) \times Ni/Fe$. The atomic $^{60}Fe/^{53}Mn$ ratio in Antarctic snow is $0.017^{+0.012}_{-0.010}$, which is more than 2 orders of magnitude higher in the case of most common chondritic abundances of Ni/Fe = 0.055 [37] than the expectation for a cosmogenic source. It is important to note here that production of ^{60}Fe is enhanced in larger meteorites because of a secondary neutron flux through spallation in the thick target [12,35]. For cosmic dust this is not the case which should reduce the expected ratio further.

To judge whether our measured ratio in the snow is significantly higher than the meteoritic ratios, we calculate the expected number of events from our sample under the assumption that the sample contains solely meteoritic radionuclides. The ratio in the snow $^{60}Fe/^{53}Mn = 0.017$ corresponds to 5 observed ^{60}Fe events. Considering the 3σ upper limit of the meteoritic ratio at the highest Ni/Fe = 1 element ratio of $(0.0019 + 3 \times 0.0002) = 0.0025$, this

would correspond to an expected number of 0.74 events. The probability that a Poisson distribution with a mean of 0.74 results in 5 or more events is only 1.0×10^{-3}. Therefore, we conclude that there is a significant enhancement of ^{60}Fe in the snow compared to interplanetary dust.

In previous studies, ^{60}Fe was detected either in geologically old deep-sea archives or in extraterrestrial objects such as meteorites or on the Moon. In this investigation, the sample material is exposed to the recent environment allowing a contribution of nuclear weapons test produced ^{60}Fe through global fallout. Thus, for the first time, global fallout ^{60}Fe has to be considered as a potential ^{60}Fe signal in environmental samples.

Nuclear reactions that could produce ^{60}Fe in significant quantities in nuclear bombs include successive (n, γ), $(n, 2n)$, (n, p), or (n, α) reactions for fast neutrons on stable elements such as Co, Ni, or Cu, and certainly double neutron capture of moderated neutrons on stable Fe. Since the contribution of all reactions to the ^{60}Fe concentration depends on the abundance and geometry of stable elements in the vicinity of the bomb test, the flux and spectrum of the neutrons which could be different for different bomb configurations as well as on the distribution behavior after the explosion, a direct calculation would be substantially model-dependent and uncertain. For this case, short-lived ^{55}Fe is used as a proxy for the ^{60}Fe production because of the analogy in reaction, abundance, and distribution behavior between the Fe isotopes.

The activation product ^{55}Fe, with a half-life of 2.7 yr [38] and references therein, could not be determined directly in Antarctic snow today after more than 20 half-lives. To estimate the amount of ^{55}Fe in Antarctica today, assuming

TABLE II. Summary of different ^{60}Fe investigations in the past. Sample material and characteristics are displayed. The range of possible ^{60}Fe fluxes into different geological and lunar reservoirs, corrected for radioactive decay and the updated half-lives, comprise values roughly between 10^{-1} and 10^{2} atoms cm^{-2} yr^{-1}. The combined value from the filter sample and the water sample for Antarctic snow is similar to the deposition into other reservoirs.

	Sample	Origin	Growth rate	^{60}Fe flux [atoms cm^{-2} yr^{-1}]
Knie et al. [12]	Ferromanganese crust	South Pacific	1–2 mm/Myr	0.5–5
Knie et al. [13]	Ferromanganese crust	Equatorial Pacific	2–3 mm/Myr	1–5
Wallner et al. [14]	Sediments	Indian Ocean	3–4 mm/kyr	20–40
	Ferromanganese crusts	Equatorial Pacific	2–5 mm/Myr	1–3
	Ferromanganese nodules	South Atlantic	2–5 mm/Myr	0.2–0.5
Ludwig et al. [15]	Sediments	Equatorial Pacific	6–19 mm/kyr	0.4–1.2
Fimiani et al. [16]	Lunar regolith	Moon	$\cdots$	20–100
This work	Surface snow	Antarctica	80 mm/yr	$1.2^{+0.6}_{-0.5}$

^{55}Fe is stable as, in principle, ^{60}Fe is over the considered timescale, the spatial and temporal distribution of global fallout have to be evaluated. The distribution of global fallout over the northern and southern hemisphere was deduced from the distribution of the fission product ^{90}Sr. The fractional deposition density of ^{90}Sr between the latitude band 70°–80° (the Kohnen Station is at 75°) is 4×10^{-3} relative to global deposition [39]. The temporal progression of global fallout could be monitored by long-lived radionuclides such as ^{90}Sr, ^{236}U, or ^{239}Pu [39–41]. The fallout of radionuclides has decreased by 4 to 5 orders of magnitude up to the mid 1980s, including fresh radionuclide input from late bomb tests. We assume a total reduction by 6 orders of magnitude until the beginning of the new millennium as it is indicated by atmospheric model calculations [39,40]. We estimate the current global fallout level of ^{55}Fe at the Kohnen Station by taking the total ^{55}Fe production from nuclear weapons tests of 1530 PBq over Earth's surface [39] and include the latitudinal global fallout distribution, obtained by the distribution of ^{90}Sr, and the temporal reduction of global fallout. The total amount of nondecaying ^{55}Fe in the latitude band 70°–80° at the present time would be 8×10^{17} atoms. This corresponds to 4×10^{5} atoms of ^{55}Fe in our sample after accounting for the total surface area of this latitude band of 11.6×10^{12} m^{2} [39] and our sampled surface area of 6.25 m^{2}. Averaging over the global scale and only taking into account the distributional behavior of the fission product ^{90}Sr, which is much less localized than the activation product ^{55}Fe and thus is more global, will overestimate the abundance of ^{55}Fe in Antarctica. Furthermore, the accumulation rate at the Kohnen Station is as low as 80 mm w.e. yr^{-1} and it is well known that the deposition rate of global fallout nuclides is proportional to the overall natural precipitation rate [42,43]. This estimation will be reduced much further for the consideration of ^{60}Fe by several additional factors. The natural isotopic abundance ratio between ^{58}Fe and ^{54}Fe of 0.05 will reduce the actual input by a factor of 20 because of less target isotope abundance.

Most importantly, the production of neutron-rich ^{60}Fe requires a double neutron capture instead of the single neutron capture for ^{55}Fe. Studies of heavy isotope abundances after thermonuclear weapons tests show in an exemplary way the rapid decrease in abundance of isotopes for every subsequent neutron capture on ^{238}U [44]. In addition, neutron-deficient ^{55}Fe is also produced by (n, α) reactions of fission neutrons on stable ^{58}Ni and dominantly by $(n, 2n)$ reactions of fusion neutrons on most abundant ^{56}Fe. The reaction ^{56}Fe$(n, 2n)^{55}$Fe is estimated to produce up to 8 times more ^{55}Fe in nuclear weapons tests than the reaction ^{54}Fe$(n, \gamma)^{55}$Fe [45], which results in less production of ^{60}Fe than estimated from ^{55}Fe. Summarizing, the production of ^{60}Fe in nuclear bomb tests and the subsequent deposition in Antarctic snow at recent times will be much lower than the measured 7.3×10^{4} atoms of ^{60}Fe and negligible.

For completeness, other possible production sites for ^{60}Fe on Earth are considered. *In situ* production is insignificant in Antarctica because of the absence of sufficient stable target elements and production through spallation on gas molecules in the atmosphere only generates lighter nuclei, since Ar is the heaviest nontrace element in the atmosphere [12]. ^{60}Fe is produced in nuclear reactors by double neutron capture on stainless steel components and dissolved Fe in the coolant, whereas superasymmetric fission of ^{235}U is not able to produce significant quantities of ^{60}Fe because of the low fission yield $< 10^{-8}$% [46]. The produced ^{60}Fe is confined within the reactor containment and so far even major nuclear accidents, such as Fukushima, do not expose measurable quantities of ^{60}Fe to the environment [47]. Nuclear reprocessing facilities discharge radionuclides, presumably including ^{60}Fe, into the oceans. Nevertheless, major reprocessing facilities like La Hague or Sellafield are located in the Northern Hemisphere, and discharges directly into the ocean should

not influence the radionuclide inventory in Antarctica. Lastly, all primordial ^{60}Fe has already decayed since the formation of Earth more than 4 Gyr ago.

By ruling out terrestrial and cosmogenic sources, we conclude that we have found, for the first time, recent ^{60}Fe with interstellar origin in Antarctica. We note, the measured recent influx into our sample is similar to the deposition into previously investigated geologically old reservoirs (Table II). The detected interstellar ^{60}Fe could originate from the LIC, which the Solar System is presently traversing. This would open a window for more detailed studies with respect to the LIC origin by additional investigation of radionuclides, mentioning only a few, like ^{92}Nb(3.5×10^7), ^{97}Tc(4.2×10^6), or ^{98}Tc$(4.2 \times 10^6$ yr), all of them are shielded by stable isobars against fission products from U on Earth. In addition, dated samples from deeper layers or even ice cores could reveal the flux of radionuclides from the LIC in the past. We would expect a sharp increase in flux of ^{60}Fe around the time when the Solar System entered the LIC, assuming the LIC is the origin of the detected ^{60}Fe. Further on, if this signal is global, as was the case for interstellar ^{60}Fe signals in the past, it should be possible to find it also in other reservoirs on Earth.

---

[*]Present address: Department of Nuclear Physics, The Australian National University (ANU), Canberra, ACT 2601, Australia.
dominik.koll@anu.edu.au

[1] E. Gruen et al., Nature (London) 362, 428 (1993).
[2] I. Mann, Annu. Rev. Astron. Astrophys. 48, 173 (2010).
[3] N. Altobelli, F. Postberg, K. Fiege, M. Trieloff, H. Kimura, V. J. Sterken, H.-W. Hsu, J. Hillier, N. Khawaja, G. Moragas-Klostermeyer, J. Blum, M. Burton, R. Srama, S. Kempf, and E. Gruen, Science 352, 312 (2016).
[4] S. Redfield and J. L. Linsky, Astrophys. J. 812, 125 (2015).
[5] J. D. Slavin, Space Sci. Rev. 143, 311 (2009).
[6] P. Frisch, J. Geophys. Res. Space Phys. 105, 10279 (2000).
[7] H. Kimura, I. Mann, and E. K. Jessberger, Astrophys. J. 582, 846 (2003).
[8] P. C. Frisch and J. D. Slavin, Short-term variations in the galactic environment of the sun, in Solar Journey: The Significance of Our Galactic Environment for the Heliosphere and Earth, edited by P. C. Frisch (Springer Netherlands, Dordrecht, 2006), pp. 133–193.
[9] D. P. Cox and R. J. Reynolds, Annu. Rev. Astron. Astrophys. 25, 303 (1987).
[10] G. Rugel, T. Faestermann, K. Knie, G. Korschinek, M. Poutivtsev, D. Schumann, N. Kivel, I. Günther-Leopold, R. Weinreich, and M. Wohlmuther, Phys. Rev. Lett. 103, 072502 (2009).
[11] A. Wallner, M. Bichler, K. Buczak, R. Dressler, L. K. Fifield, D. Schumann, J. H. Sterba, S. G. Tims, G. Wallner, and W. Kutschera, Phys. Rev. Lett. 114, 041101 (2015).
[12] K. Knie, G. Korschinek, T. Faestermann, C. Wallner, J. Scholten, and W. Hillebrandt, Phys. Rev. Lett. 83, 18 (1999).
[13] K. Knie, G. Korschinek, T. Faestermann, E. A. Dorfi, G. Rugel, and A. Wallner, Phys. Rev. Lett. 93, 171103 (2004).
[14] A. Wallner, J. Feige, N. Kinoshita, M. Paul, L. K. Fifield, R. Golser, M. Honda, U. Linnemann, H. Matsuzaki, S. Merchel, G. Rugel, S. G. Tims, P. Steier, T. Yamagata, and S. R. Winkler, Nature (London) 532, 69 (2016).
[15] P. Ludwig, S. Bishop, R. Egli, V. Chernenko, B. Deneva, T. Faestermann, N. Famulok, L. Fimiani, J. M. Gómez-Guzmán, K. Hain, G. Korschinek, M. Hanzlik, S. Merchel, and G. Rugel, Proc. Natl. Acad. Sci. U.S.A. 113, 9232 (2016).
[16] L. Fimiani, D. L. Cook, T. Faestermann, J. M. Gómez-Guzmán, K. Hain, G. Herzog, K. Knie, G. Korschinek, P. Ludwig, J. Park, R. C. Reedy, and G. Rugel, Phys. Rev. Lett. 116, 151104 (2016).
[17] N. Benitez, J. Maiz-Apellaniz, and M. Canelles, Phys. Rev. Lett. 88, 081101 (2002).
[18] T. Berghoefer and D. Breitschwerdt, Astron. Astrophys. 390, 299 (2002).
[19] D. Breitschwerdt and M. A. de Avillez, Astron. Astrophys. 452, L1 (2006).
[20] D. Breitschwerdt, J. Feige, M. M. Schulreich, M. A. de. Avillez, C. Dettbarn, and B. Fuchs, Nature (London) 532, 73 (2016).
[21] M. M. Schulreich, D. Breitschwerdt, J. Feige, and C. Dettbarn, Astron. Astrophys. 604, A81 (2017).
[22] E. E. Mamajek, Proc. Int. Astron. Union 10, 21 (2015).
[23] B. J. Fry, B. D. Fields, and J. R. Ellis, Astrophys. J. 827, 48 (2016).
[24] T. Athanassiadou and B. Fields, New Astron. 16, 229 (2011).
[25] H. Yang and M. Ishiguro, Astrophys. J. 813, 87 (2015).
[26] M. Honda and M. Imamura, Phys. Rev. C 4, 1182 (1971).
[27] R. Trappitsch and I. Leya, Meteorit. Planet. Sci. 48, 195 (2013).
[28] B. Medley, J. R. McConnell, T. A. Neumann, C. H. Reijmer, N. Chellman, M. Sigl, and S. Kipfstuhl, Geophys. Res. Lett. 45, 1472 (2018).
[29] S. Merchel and U. Herpers, Radiochim. Acta 84, 215 (1999).
[30] M. Poutivtsev, I. Dillmann, T. Faestermann, K. Knie, G. Korschinek, J. Lachner, A. Meier, G. Rugel, and A. Wallner, Nucl. Instrum. Methods Phys. Res., Sect. B 268, 756 (2010).
[31] D. Koll, Search for recent ^{60}Fe deposition in Antarctica with AMS, Master's thesis, Technical University of Munich, 2018.
[32] D. Koll, C. Busser, T. Faestermann, J. Gómez-Guzmán, K. Hain, A. Kinast, G. Korschinek, D. Krieg, M. Lebert, P. Ludwig, and F. Quinto, Nucl. Instrum. Methods Phys. Res., Sect. B 438, 180 (2019).

[33] G. J. Feldman and R. D. Cousins, Phys. Rev. D **57**, 3873 (1998).

[34] K. Knie, S. Merchel, G. Korschinek, T. Faestermann, U. Herpers, M. Gloris, and R. Michel, Meteorit. Planet. Sci. **34**, 729 (1999).

[35] S. Merchel, T. Faestermann, U. Herpers, K. Knie, G. Korschinek, I. Leya, R. Michel, G. Rugel, and C. Wallner, Nucl. Instrum. Methods Phys. Res., Sect. B **172**, 806 (2000).

[36] U. Ott, S. Merchel, S. Herrmann, S. Pavetich, G. Rugel, T. Faestermann, L. Fimiani, J. M. Gomez-Guzman, K. Hain, G. Korschinek, P. Ludwig, M. D'Orazio, and L. Folco, Meteorit. Planet. Sci. **49**, 1365 (2014).

[37] H. Palme, K. Lodders, and A. Jones, in *Treatise on Geochemistry*, 2nd ed., edited by H. D. Holland and K. K. Turekian (Elsevier, Oxford, 2014), pp. 15–36.

[38] S. Pomme, H. Stroh, and R. V. Ammel, Appl. Radiat. Isot. **148**, 27 (2019).

[39] UNSCEAR 2000 Report to the General Assembly, Scientific Committee on the Effects of Atomic Radiation, Volume I: Sources, Annex C: Exposures from man-made sources of radiation, page 157 (2000), ISBN 92-1-142238-8.

[40] S. R. Winkler, P. Steier, and J. Carilli, Earth Planet. Sci. Lett. **359–360**, 124 (2012).

[41] S. Olivier, S. Bajo, L. K. Fifield, H. W. Gäggeler, T. Papina, P. H. Santschi, U. Schotterer, M. Schwikowski, and L. Wacker, Environ. Sci. Technol. **38**, 6507 (2004).

[42] S. E. Palsson, B. J. Howard, and S. M. Wright, Sci. Total Environ. **367**, 745 (2006).

[43] G. L. Roux, C. Duffa, F. Vray, and P. Renaud, Journal of Environmental Radioactivity **101**, 211 (2010).

[44] H. Diamond, P. R. Fields, C. S. Stevens, M. H. Studier, S. M. Fried, M. G. Inghram, D. C. Hess, G. L. Pyle, J. F. Mech, W. M. Manning, A. Ghiorso, S. G. Thompson, G. H. Higgins, G. T. Seaborg, C. I. Browne, H. L. Smith, and R. W. Spence, Phys. Rev. **119**, 2000 (1960).

[45] C. T. Hoang, Study of the fallout of artificial iron-55 application to the evaluation of the fallout of natural iron of stratospheric origin, Ph. D. thesis, 1969.

[46] K. Knie, A. Elhardt, T. Faestermann, G. Korschinek, C. Lierse, G. Rugel, and A. Stippschild, Nucl. Phys. **A723**, 343 (2003).

[47] B. L. Rosenberg, J. E. Ball, K. Shozugawa, G. Korschinek, M. Hori, K. Nanba, T. E. Johnson, A. Brandl, and G. Steinhauser, Appl. Geochem. **85**, 201 (2017).